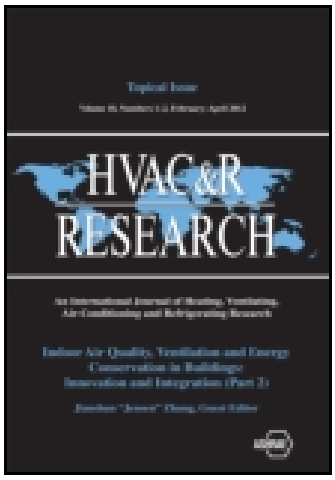

HVAC&R Research
Publication details, including instructions for authors and subscription information:
http://www.tandfonline.com/loi/uhvc20

Developing empirical correlations for frost thickness and air face velocity degradation for microchannel heat exchangers used in heat pump applications under frosting conditions

Ehsan Moallem [a], Tommy Hong [a], Lorenzo Cremaschi [a] & Daniel E. Fisher [a]
[a] School of Mechanical and Aerospace Engineering, Oklahoma State University, Stillwater, OK, 74078, USA
Accepted author version posted online: 08 Jul 2013.Published online: 25 Oct 2013.

To cite this article: Ehsan Moallem, Tommy Hong, Lorenzo Cremaschi & Daniel E. Fisher (2013) Developing empirical correlations for frost thickness and air face velocity degradation for microchannel heat exchangers used in heat pump applications under frosting conditions, HVAC&R Research, 19:7, 779-787

To link to this article: http://dx.doi.org/10.1080/10789669.2013.812500

HVAC&R Research (2013) **19**, 779–787

ISSN: 1078-9669 print / 1938-5587 online
DOI: 10.1080/10789669.2013.812500

Taylor & Francis
Taylor & Francis Group

Developing empirical correlations for frost thickness and air face velocity degradation for microchannel heat exchangers used in heat pump applications under frosting conditions

EHSAN MOALLEM*, TOMMY HONG, LORENZO CREMASCHI, and DANIEL E. FISHER

School of Mechanical and Aerospace Engineering, Oklahoma State University, Stillwater, OK 74078, USA

This study experimentally investigated the frost growth on louvered folded fins in outdoor microchannel heat exchangers used in air-source heat pump systems. The effects of surface temperature and fin geometries on the performance of the microchannel heat exchangers under frosting condition were studied. Seven fin samples with various fin widths, fin heights, and fin densities and a louver angle of approximately 30° were tested in controlled laboratory conditions that replicated those of actual heat pump systems in the winter season. The fin surface temperature was experimentally measured with the novel methodology developed in the present study. Experimental data of local frost thickness, air pressure drop across the coils, time of frost–defrost cycles, and heat transfer rates were recorded for heat exchangers operating in actual transient frosting conditions. Data showed that frosting time and frost growth rates depended mainly on the local fin surface temperature. A set of empirical correlations were developed to predict the frost thickness on the fin leading edge and the reduction of air face velocity due to air pressure drop across the frosted coil during frosting operation. The correlations were compared against experimental data of frost collected in the present study, and satisfactory agreement was achieved. The frost thickness correlation and air face velocity correlations aid in the calculation of the instantaneous air-side Reynolds numbers during frosting operation of the fin samples. These are critical for predicting the heat transfer rates of the microchannel coils in quasi-steady-state frosting operating conditions.

Introduction

Air-source heat pump systems are used for heating and cooling residential and commercial buildings all year around. They are energy efficient and have low installation costs. An air-source heat pump exchanges heat directly from the indoor environment to the outdoor ambient air, and during winter operation, the outdoor coil might accumulate frost on its surface. Defrost cycles need to be periodically executed in between the heating cycles to dispose of the accumulated frost on the surface of heat exchanger. Microchannel coils have been employed recently in heat pump applications to replace conventional fin and tube coils due to their compactness, lower coil weight, and less refrigerant charge, which could lower the direct contribution to global warming due to potential refrigerant leakage (Garimella 2003; Kim and Groll 2003; Kim and Bullard 2002; Park and Hrnjak 2007). During heating mode, the energy performance of heat pump systems with microchannel outdoor coils are generally low due to a higher frequency of defrost cycles (Kim and Groll 2003; Padhmanabhan et al. 2008).

Received December 6, 2012; accepted May 23, 2013
Ehsan Moallem, PhD, Associate Member ASHRAE, is Lecturer. **Tommy Hong** is Research Engineer. **Lorenzo Cremaschi, PhD**, Member ASHRAE, is Associate Professor. **Daniel E. Fisher, PhD, PE**, Fellow ASHRAE, is Professor.
*Corresponding author e-mail: moallem@okstate.edu

There are several parameters that affect frost formation on outdoor coils, such as air velocity, air humidity, air temperature, cold surface temperature (Kondepudi and O'Neal 1989; Lee et al. 1997), surface energy and fin-base surface microscopic characteristics (including coatings and roughness; Na and Webb 2003; Shin et al., 2003), fin geometry, and coil water retention after defrost cycles (Xia et al. 2006).

Kim and Groll (2003) studied two microchannel geometries with different fin densities and coil orientations under frosting conditions and concluded that water drainage and refrigerant distribution in headers needed to be improved for achieving a better frosting performance. Xia et al. (2006) experimentally investigated five louvered-fin flat tube microchannel evaporators and observed that water retention has a significant effect on the air pressure drop in subsequent cycles. In another study, Zhang and Hrnjak (2010) investigated the frosting performance of parallel-flow parallel-fin (PF^2) flat tube microchannel heat exchangers with horizontally installed tubes. The authors observed an improvement in frosting performance over a conventional serpentine fin that was attributed to the better drainage capability of the PF^2 heat exchanger. Padhmanabhan et al. (2008), on the other hand, observed that removing the water residual at the end of the defrost cycle by flushing the microchannel coil with pressurized nitrogen improved the next frost cycle time by only 4%. The preliminary results of this study (Moallem et al. 2012c) also showed that water retention, which was assumed to be one of the main reasons of faster frost growth on microchannels, is not the

dominant factor affecting the frost, even though it seems to have some effects on the air side pressure drop. The key parameters that affect frost nucleation and growth were observed to be fin surface temperature (Moallem et al. 2012c) and the fin geometry. In several previous studies on microchannel heat exchanger in the literature, the geometries were varied to search for the best option for thermal performance. As a result, the effect of geometry modification was coupled with the effect of surface temperature change. To isolate and study the effect of surface temperature, a new methodology was developed by the authors that measured and controlled the fin surface temperature independently and isolated its effects from the geometry effects (Moallem et al. 2013). The experimental data of authors' previous work are used in the present study.

Although a number of studies are available on frosting behavior of microchannels, their findings are restricted to a limited number of geometries tested. The essence of developing an empirical correlation aims to unite previous findings into a general form that could be employed for a variety of geometries. There are correlations in the literature that can predict the heat transfer coefficient and pressure drop for various micrchannel geometries in steady-state dry and steady-state wet conditions, but there have been no correlations to predict the performance of microchannel coils under frosting conditions. Previous researchers developed models for frost growth that might be difficult to implement, had convergence issues, and/or required advanced skills for troubleshooting, long hours of computational time, and extensive experimental validation of the model. In addition, the predicted results from the current models available in the public domain are sometimes contradicting or inconsistent with each other. The most important correlations that would be needed are for the frost thickness, instantaneous air face velocity, and instantaneous heat transfer coefficient. In the present study, new correlations for frost thickness correlation and reduction of the air face velocity are developed and discussed. The correlations were verified against experimental data. The scientific merit of this work is a fundamental understanding of frost growth, which changes the air-side hydraulic geometry for the various geometries of folded louvered fins of microchannel heat exchangers. Once the instantaneous hydraulic geometry and air velocity are determined during the frost period, the Reynolds numbers are calculated. These numbers could be used for the development of instantaneous heat transfer coefficients during frosting operations, which is a future extension of this work.

Experimental setup

The fin samples are one column of louvered fins (15 cm in length) cut from commercially available microchannel coils. The tubes of this one column were eliminated, and heat conduction was adopted in cooling the samples. This approach helped to eliminate the effect of different internal tube designs and microchannel ports and ensured a uniform one-dimensional conduction heat transfer. A typical fin sample and schematic can be seen in Figure 1; the detailed geometry of the samples is shown in Table 1. The samples had a broad range of fin densities, depths, widths, and heights, while the louver angle was approximately 30° for all samples.

In order to remove the heat from the sample fin, or cool it to the desired temperature, a method originally proposed by Thomas et al. (1999) was used. Thermoelectric cooling (TEC) modules were installed in each side of the samples to remove the heat and control the fin temperature, as shown in Figure 2. With this configuration, thermocouples at the base of the fins samples showed constant temperatures of about –5°C, –8°C, and –11°C in each test. An airflow test setup

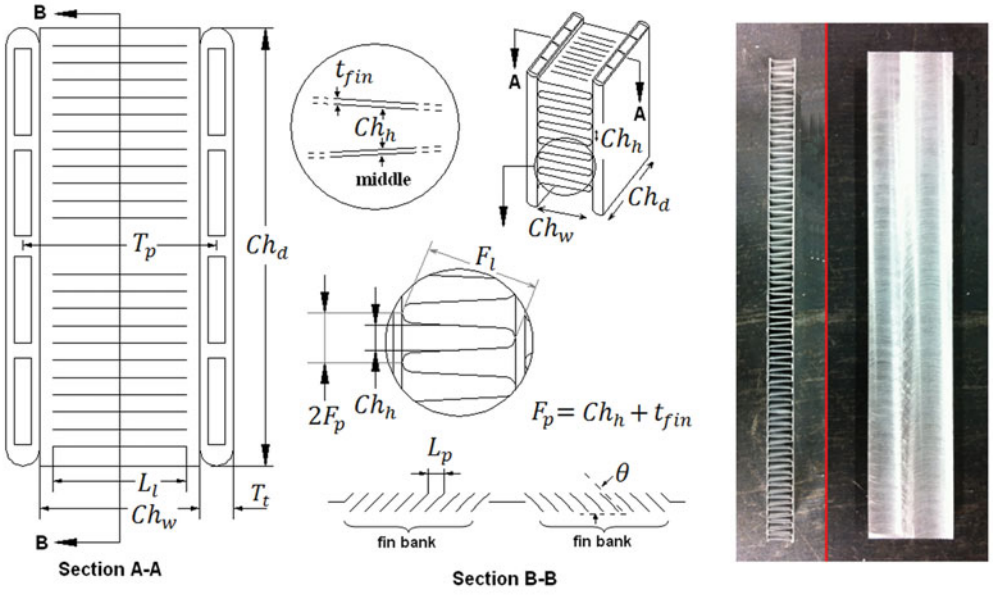

Fig. 1. Schematic drawing of a microchannel sample with geometrical parameters shown in the left side of the figure. One of the fin samples is shown on the right side of the figure. These drawings were made at Oklahoma State University and were not given by the manufacturers (color figure available online).

Table 1. Details of geometries of microchannel fin samples used in present study.

Sample no.	Fin depth (Ch_d), mm	Fin width (Ch_w), mm	Channel height (Ch_h), mm	Fin density, FPI	Tube thickness, mm	Fin thickness, mm	Fin type	Number of louvers	Louver pitch, mm	Louver angle, degrees	Louver height, mm	Louver length, mm
1	27.0	8.0	2.34	10.4	1.8	~ 0.1	Flat fin corrugated	—	—	—	—	—
2	27.0	8.0	1.77	13.6	1.8	~ 0.1	Louvered	16	1.50	~30	0.22	6.5
3	26.0	7.6	1.15	20.3	1.4	~ 0.1	Louvered	24	0.94	~30	0.09	6.0
4	25.0	10.0	1.21	19.4	1.7	~ 0.1	Louvered	18	1.22	~30	0.24	7.5
5	25.0	13.0	1.20	19.6	2.0	~ 0.1	Louvered	20	1.23	~30	~ 0.21	9.5
6	30.0	8.1	1.27	18.5	1.4	~ 0.1	Louvered	28	0.86	~30	~ 0.2	7.0
7	19.0	8.0	1.36	17.4	3.0	~ 0.1	Louvered	16	0.94	~30	~ 0.2	6.5

was designed and built in the laboratory to control the test condition specified in AHRI Standard 210/240 (2008) for heat pump system performance rating. The apparatus and the vice that holds the sample were placed inside a large air tunnel, as shown in step 4 at the top and component 2 at the bottom of Figure 2. The tunnel is a closed-loop duct system equipped with ultrasonic humidifiers, a refrigeration coil, an electrical heater, and a centrifugal variable-speed fan. The inlet air is controlled at 1.67°C/0.56°C (35°F/33°F) dry-bulb/wet-bulb temperature (~82% RH).

All experimental tests were conducted with the fin sample initially in a dry condition. Each test started with air at 1.5 m/s face velocity on fin samples. Fan was kept at a constant RPM throughout the entire test, and air face velocity was allowed to drop. This method of testing was preferred over a constant air velocity method since it was closer to the actual operation of the outdoor evaporator coils in air-source heat pump systems. The air tunnel had had a cross-section of 1 ft by 1 ft (0.3 m by 0.3 m), and the location of test apparatus was carefully chosen to be away from cooling or heating coils to allow a uniform temperature and velocity distribution on the sample. It should also be noted that only a small part of total airflow (about 5 cfm (0.0024 m^3/s)) was diverted to the small microchannel samples, while the rest of the flow (about 100 cfm (0.047 m^3/s)) was recirculated and bypassed the fin sample. Thus, when reducing 5 cfm (0.0024 m^3/s) for the sample to 0 cfm, the rest of the flow was practically unaffected and the working conditions of the fan in the test setup were not drastically influenced during the frosting tests of the present work. More details about experimental setup can be found in Hong et al. (2012).

Frost thickness was measured with a magnifying high resolution charge-coupled device (CCD) camera that has a

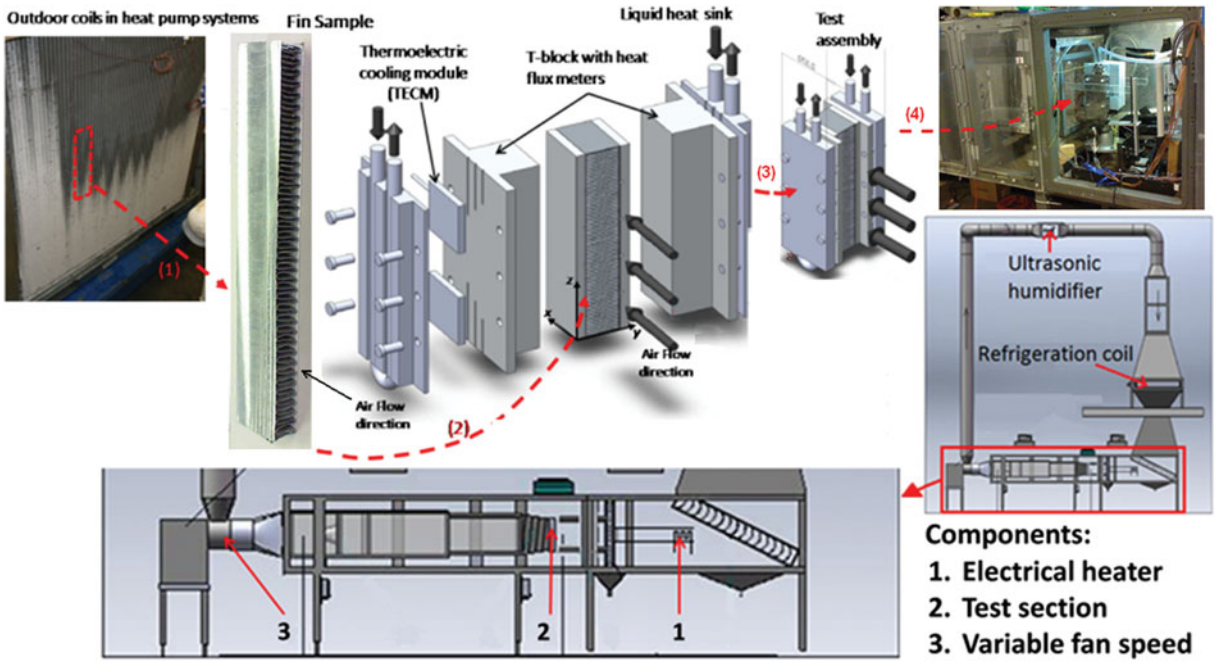

Fig. 2. Procedure for preparation of test assembly setup inside wind tunnel (top) and schematic of air tunnel or airflow loop (bottom) (color figure available online).

borescope probe. The value of frost thickness was obtained by scaling high-resolution images using special imaging computer software (iView PC) with an accuracy of ±0.03 mm. The uncertainty was calculated using uncertainty propagation calculation, which showed 12% on the air side and 8% on the conduction side. More details about the instrumentation and test procedures are in Hong (2011) and Hong et al. (2012). The verifications of the instrumentation connectivity, accuracy, and validation of proper data recording were demonstrated through a set of validation tests called calorimeter tests. Experimental validation tests included heat balance verification (two methods of the air enthalpy method versus conduction heat transfer), performed on all of the fin samples, which showed the difference never exceeded 15% in dry tests and during quasi-steady-state periods of the frosting tests (Moallem et al. 2012b).

Results and discussion

Visual observations

The frost growth pattern on microchannel fin sample 2 is shown in Figure 3. Similar results were observed for other samples (Moallem et al. 2013). The location of the camera was in the center of the 6-in.-long sample. Figure 3 shows the frost accumulation over time; the frost time is measured from the time the airflow was started on the cold sample to the end of the frosting period, that is, when the air face velocity reached 30% of its initial value. There were not significant visual differences between the frost layers that grow on different geometries. The end of the cycle occurred at a time when the air gaps between the fins were almost completely blocked by frost.

Frost empirical correlation, scope and fundamentals

The effect of various surface temperatures and geometries were previously published in previous work (Moallem et al. 2013). In this section, a new set of frost correlations were developed and verified against experimental data. The fundamental frost formation theories in the literature associated the frost formation rate with the vapor pressure of the air and temperature at which frost forms, which is basically the surface temperature. In crystallization theory, for the phase transition of the water vapor into ice crystals, air should be in a supersaturation level. Air supersaturation (this article refers to this quantity as frost number, *Fs*) is the driving force for migration of water vapor particles and their deposition on the cold surface, which is defined as the following (Na and Webb 2004; Sanders 1974):

$$Fs = S = \frac{P_{air} - P_{surf}}{P_{surf}}, \tag{1}$$

$$\delta = f(t_t, T_{surf}, T_{air}, \omega_{air}, Geometry) \Rightarrow$$

$$\delta = f(\mathrm{Fo}, Fs, Geometry) Geometry: Ch_w, Ch_h, Ch_d, \tag{2}$$

$$\delta = \frac{t}{(Ch_h/2)}, \tag{3}$$

$$\mathrm{Fo} = \frac{D_{ab} t_t}{Ch_h^2}, \tag{4}$$

where δ is the dimensionless frost thickness and is unity when the free-flow area between two adjacent fins is completely blocked by frost. Fo or Fo_m, which is the mass transfer Fourier number or dimensionless time, is defined according to Equation 4. As the data of Figure 4 shows, the frost thickness starts from 0 at the beginning of the test and reaches near 1 at the end. For geometry parameters, it was observed that except a few discrepancies, three parameters of fin pitch (Ch_h), fin length (Ch_w), and fin depth (Ch_d) (as shown in Figure 1) could predict the experimental data with sufficient accuracy.

Frost thickness correlation

In order to predict the frosting behavior of microchannels, it should be pointed out that the air-side free-flow geometry changes during the frost period. This observation is the key to calculating the correct instantaneous Reynolds number in quasi-steady-state operation. Although the frost thickness was measured only at the leading edge, this parameter is sufficient to calculate the critical Reynolds number, which is the Re number estimated at the minimum cross-sectional area. It was concluded during this study that some of the geometrical parameters in the frost thickness correlation had to be in dimensional form in order to provide better accuracy of correlation when compared to the experimental data. Minimizing root mean square (RMS) errors was the approach taken to find the coefficients of the correlation, which is as follows:

$$\delta = \alpha \mathrm{Fo}^{\beta}, \tag{5}$$

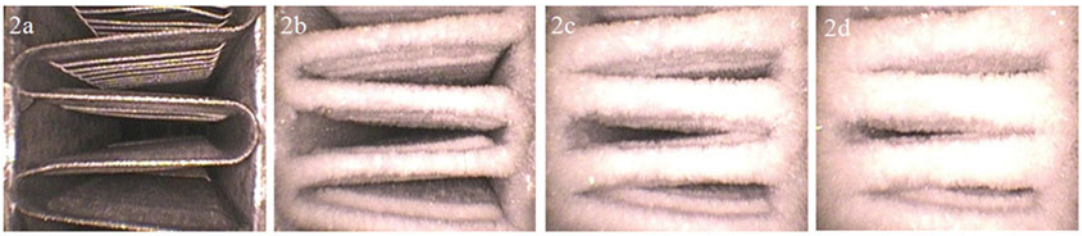

Fig. 3. Microchannel sample 2 under frosting conditions; a, b, c and d represent time of 0, 8, 16 and 24 minutes after starting the test. $T_{surf} = -8°C$ (18°F) and air temperature = 1.7°C/0.6°C (35°F/33°F) db/wb. Similar visual results were observed for surface temperatures of −5°C (23°F) and −11°C (12°F) with different time duration (color figure available online).

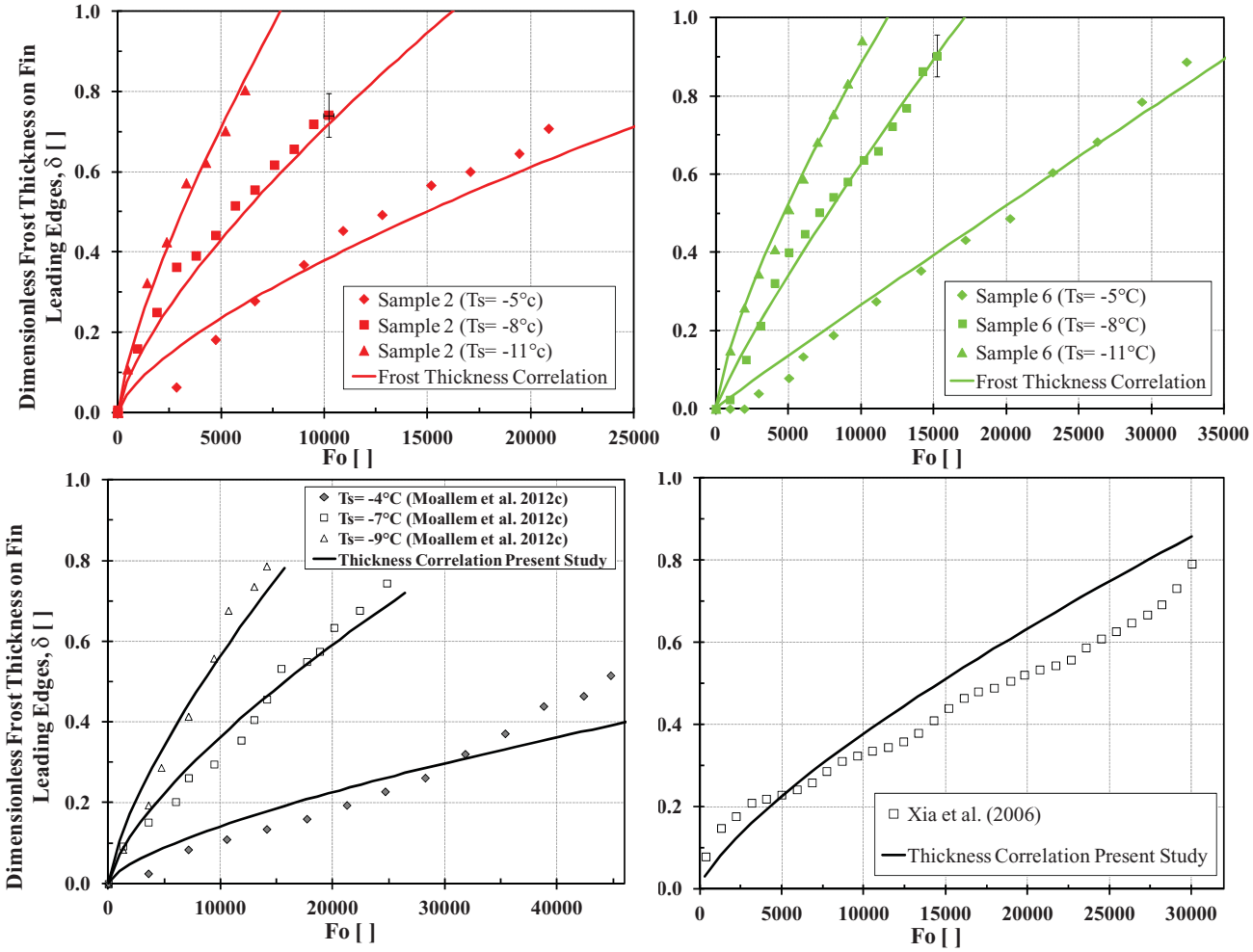

Fig. 4. Frost thickness correlation versus experimental measured frost thickness data for sample 2 and 6 (top). Similar results were observed for other samples. Comparison of present correlation with previous published works Moallem et al. (2012c and Xia et al. (2006) (bottom) (color figure available online).

$$\alpha = \left(\frac{1}{\beta^{5.5}}\right)\{(c_1 Ch_w^2 + c_2 Ch_w + c_3)(c_4 Ch_h^2 + c_5 Ch_h + c_6) \times (c_7 Ch_d^2 + c_8 Ch_d + c_9)(Fs - c_{10}) + (c_{11} Ch_w^2 + c_{12} Ch_w + c_{13})(c_{14} Ch_h^2 + c_{15} Ch_h + c_{16}) \times (c_{17} Ch_d^2 + c_{18} Ch_d + c_{19})\}, \quad (6)$$

$$\beta = 0.75 + (c_{20} Ch_w^2 + c_{21} Ch_w + c_{22})(c_{23} Ch_h^2 + c_{24} Ch_h + c_{25}) \times (c_{26} Ch_d^2 + c_{27} Ch_d + c_{28})(Fs - c_{10}). \quad (7)$$

In the above equations, α and β are functions of geometry and Frost number; α ranges from $1.2E{-}5$ to $1.9E{-}3$, and β varied from 0.55 to 0.99. Ch_h, Ch_w, and Ch_d have dimensions in millimeters. Coefficients c_1 to c_{28} are constants, and their values are shown in Table 2. Equation 5 was able to capture the experimental data of frost thickness on 21 different pieces of frost data that included 7 different geometries tested at 3 fin surface temperatures. A comparison of the instantaneous frost predicted by using Equation 5 versus experimental thickness data for sample 6 and sample 2 at three temperatures is shown in Figure 4. Similar results were observed for other geometries (Figure 5).

The developed correlation was also compared to other experimental microchannel frost thickness data with larger 1 ft

Table 2. Coefficients of geometry in general frost thickness correlation.

c_1	$-2.24444E{-}06$	c_6	$-2.16158E+00$	c_{11}	$-3.82446E{-}07$	c_{16}	$-1.62560E+00$	c_{21}	$-5.555E{-}01$	c_{26}	$-1.099E{-}02$
c_2	$4.34942E{-}05$	c_7	$2.47364E{-}03$	c_{12}	$-6.77335E{-}06$	c_{17}	$-2.86864E{-}03$	c_{22}	$4.275E+00$	c_{27}	$5.164E{-}01$
c_3	$-7.89706E{-}05$	c_8	$-1.03390E{-}01$	c_{13}	$2.58664E{-}04$	c_{18}	$1.33878E{-}01$	c_{23}	$1.619E+00$	c_{28}	$-5.848E{+}00$
c_4	$-1.22951E+00$	c_9	$1.96625E+00$	c_{14}	$-9.36590E{-}01$	c_{19}	$-5.38708E{-}01$	c_{24}	$-5.678E+00$		
c_5	$4.16146E+00$	c_{10}	$1.36432E+00$	c_{15}	$3.35870E+00$	c_{20}	$1.28500E{-}02$	c_{25}	$6.102E+00$		

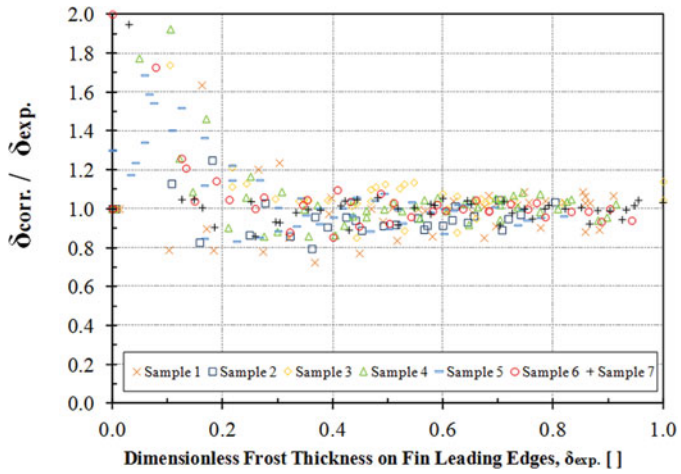

Fig. 5. Frost thickness correlation versus experimental measured dimensionless frost thickness data for samples 1–7 (color figure available online).

by 1 ft (0.3 m by 0.3 m) microchannel coils (Moallem et al. 2012a), and the result was in satisfactory agreement, as shown in Figure 4. Also, the present form of correlation was compared against frost thicknesses data obtained in Xia et al. (2006), where a different experimental setup was used to measure frost growth. The frost thickness correlation developed in this work, however, captured well the trend of the data, as shown in Figure 4. It should be emphasized that coefficients c_1 to c_{28} in Table 2, which were based only on the measurements of Hong et al. (2012), were not tuned to fit the experimental results of Moallem et al. (2010) and Xia et al. (2006).

The overall performance of frost correlation is shown in Figure 5 in which frost thickness ratios $\delta_{correlation}/\delta_{experimental}$ are shown on vertical axis versus the actual frost thickness measurement data. The correlation seems to be able to predict the experimental frost thickness reasonably well for all data; however, there are some data points that have significant deviation from correlation prediction when the frost thickness ratio is less than 0.2. This is due to the early condensation frosting or formation of supercooled droplets, which delayed frost growth process at early stages of growth as discussed in detail in previous studies (Hoke et al. 2004; Moallem et al. 2012a; Na and Webb 2003). These points acted like singularity points and created division by zero, and thus large errors, in the analysis.

Error analysis was performed on the present frost thickness correlation and relative errors, and RMS errors are reported in Table 3. The relative error indicates that the frost thickness correlation can predict the experimental data within a certain average percentage of accuracy calculated according to the following:

$$Relative\ error = \frac{1}{n}\sum \frac{ABS(\delta_{correlation} - \delta_{experimental})}{\delta_{experimental}} \times 100,$$

$$RMS\ error = \sqrt{\frac{1}{n}\sum \left(\frac{\delta_{correlation} - \delta_{experimental}}{\delta_{experimental}}\right)^2} \times 100, \quad (8)$$

where n is the total number of data points, which is 320 in the present study. RMS error was calculated using the same approach. As the data in Table 3 show, the present frost thickness correlation predicts the entire set of experimental data with average ±17.6% accuracy. As previously discussed, by eliminating the points of singularity for which frost has near-zero values, the correlation can predict 95% of the thickness experimental data within an average of ±9.8% accuracy.

Air face velocity degradation correlation

In dry and wet microchannel coils, the geometry can be assumed to be fixed, and steady-state conditions are sound. In frosting conditions, the geometry is changing at each moment, and the velocity is the result of the pressure balance across the coil and of the additional resistance created by frost buildup on the coil surfaces. As the frost grows, the free-flow area between fins is reduced. The increased air pressure drop causes a major reduction in air face velocity. It is also possible to force the air face velocity to remain constant all through a frost test by increasing the fan rotational speed and power. This second approach is quite different from the actual operation of outdoor coils of air-source heat pumps. In addition, calculations showed that forcing the air face velocity to be constant would cause the local air velocity between the frosted fins to increase more than ten times with respect to initial dry conditions. It was concluded that constant air face velocity would provide unrealistic heat transfer coefficients and very large heat transfer rates, as discussed in more detail in Moallem et al. (2012a, 2012d).

When frost started to deposit on the surface, it formed a frost layer with considerable thickness on the fin surface, as shown in Figure 4. The air pressure drop across the microchannel increased considerably (Moallem et al. 2012b). With increasing pressure drop, the total airflow rate was affected, and the air face velocity on the microchannel sample decreased. For every value of air pressure drop across the microchannel

Table 3. Error analysis for thickness correlation.

Error	Sample 1	Sample 2	Sample 3	Sample 4	Sample 5	Sample 6	Sample 7	70% of entire database	80% of entire database	90% of entire database	95% of entire database	Entire database
δ predicted within average of ±, %	17.4	11.5	26.4	29.0	16.4	16.2	6.5	4.3	5.2	7.2	9.8	17.6
RMS error, %	50.4	21.5	34.7	38.8	28.4	28.2	13.4	—	—	—	—	30.8

Table 4. Coefficients of geometry in general frost air face velocity correlation.

c_1	2.36032*E*–02	c_6	5.90549*E*–08	c_{11}	9.29921*E*–01	c_{16}	1.12464*E*–01	c_{21}	4.46048*E*–03	c_{26}	–7.70151*E* + 01
c_2	–5.50886*E*–01	c_7	9.37121*E*–04	c_{12}	–3.22532*E* + 00	c_{17}	–1.92793*E*–01	c_{22}	–6.67660*E* + 00	c_{27}	2.50000*E* + 00
c_3	3.74068*E* + 00	c_8	–3.02470*E*–02	c_{13}	–3.31519*E*–01	c_{18}	–2.08972*E*–06	c_{23}	9.30292*E* + 00	c_{28}	6.00000*E*–05
c_4	2.22105*E*–08	c_9	1.24149*E* + 00	c_{14}	2.40261*E* + 00	c_{19}	4.74618*E*–05	c_{24}	–1.22558*E*–01		
c_5	–7.95832*E*–08	c_{10}	–4.68794*E*–02	c_{15}	–2.63953*E*–03	c_{20}	–2.55006*E*–04	c_{25}	6.16741*E* + 00		

sample during the frosting test, one value of corresponding air face velocity was measured. The objective of the correlation developed in the present study was to correlate the change of the air face velocity entering the microchannel sample with frost thickness, fin geometric dimensions, and time, as shown in Equations 9–12:

$$\text{Normalized velocity}_{(\text{correlation})} = \frac{V_{air,face}}{V_{air,face_0}} = a\text{Fo}^2 + b\text{Fo} + 1, \tag{9}$$

$$a = \left(c_1 Ch_w^2 + c_2 Ch_{w+} c_3\right)\left(c_4 Ch_h^2 + c_5 Ch_h + c_6\right) \times \left(c_7 Ch_d^2 + c_8 Ch_{d+} c_9\right)(Fs)^{p_1}, \tag{10}$$

$$p_1 = \left(c_{10} Ch_w^2 + c_{11} Ch_{w+} c_{12}\right)\left(c_{13} Ch_h + c_{14}\right) \times \left(c_{15} Ch_d^2 + c_{16} Ch_{d+} c_{17}\right), \tag{11}$$

$$b = \left(c_{18} Ch_w^2 + c_{19} Ch_{w+} c_{20}\right)\left(c_{21} Ch_h^2 + c_{22} Ch_h + c_{23}\right) \times \left(c_{24} Ch_d^2 + c_{25} Ch_{d+} c_{26}\right)(Fs)^{c_{27}} + c_{28}. \tag{12}$$

In the above equations, a and b are functions of fin geometry and Fs number, and p_1 is the power of the frost number. There are a set of constants that are shown in Table 4. Ch_h, Ch_w, and Ch_d are in millimeters. The present form of velocity correlation predicted the velocity reduction on the seven different geometries with three different surface temperatures. The result for microchannel sample 6 is shown in Figure 6. Similar results were obtained for other samples (see Figure 7). The overall performance of velocity correlation in Equation 9 is shown in Figure 7. There is a concentration of data points on the right side of the horizontal axis where the normalized experimental air face velocity is near 1. Figure 7 also shows that for near the end of the test, where the air velocities are low, the error percentage increases. These points were the points when the velocities were very low. As shown in Figure 6, while the correlation does not fail to predict the experimental data at the end of each frost test, the magnitude of velocity is small and a large percentage of error occurs.

Figure 7 shows that the concentration of data points is not uniform all through the horizontal axis. The data points have been collected in equal time intervals in the frost test. However, as the air velocity is near initial velocity for a considerable time of the test, as shown in Figure 6, the concentration of data points are grouped more around 1 in the horizontal axis of Figure 7. A small percentage of the data points were located outside 10% accuracy of the present correlation according to the following analysis. Table 5 provides a summary of the statistical error when using the correlation (Equation 9) for predicting the experimental velocity data. The errors in Table 5 are calculated for 375 data points in 21 frost tests for 7 geometries of the present study; each geometry was run at three different fin surface temperatures. The error was calculated in the same method as previously described regarding the thickness correlation. Data shows that the velocity correlation can predict the entire set of data with an average error of 7.7%.

The rate of change of the air face velocity did not depend only on air pressure drop through the microchannel but also on the fan curve and system resistance due to the duct and other components of the test setup. In the present study, the blower

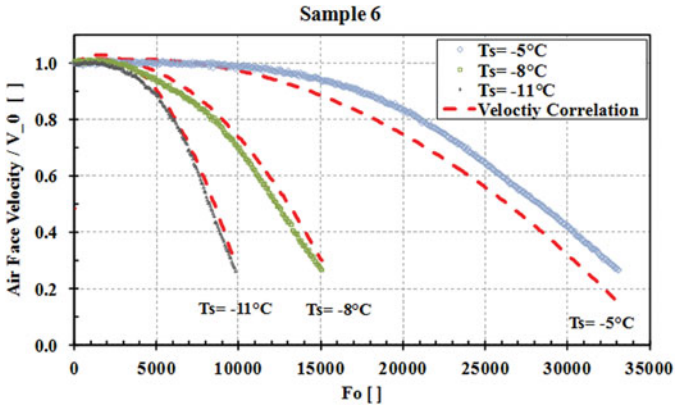

Fig. 6. Air face velocity drop correlation versus experimental measured air face velocity data sample 6; similar results were observed for other samples (color figure available online).

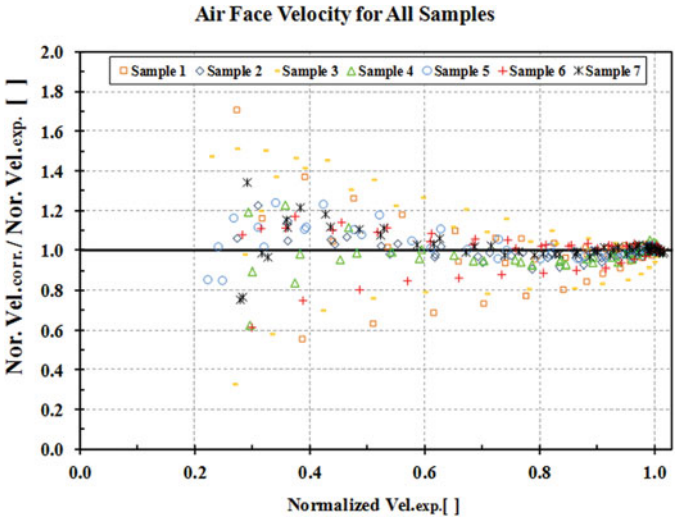

Fig. 7. Frost air face velocity correlation versus normalized experimental measured air face velocity data for samples 1–7 (color figure available online).

Table 5. Error analysis of velocity correlation

Error	Sample 1	Sample 2	Sample 3	Sample 4	Sample 5	Sample 6	Sample 7	70% of entire database	80% of entire database	90% of entire database	95% of entire database	Entire database
Nor. air vel. predicted within average of ± [%]	9.2	3.1	21.6	4.6	4.8	6.2	4.7	3.2	3.9	5.4	6.2	7.7
RMSeError [%]	15.0	4.8	34.7	7.5	7.2	8.7	8.5	—	—	—	—	12.3

used during the experiments was representative of a mid-class well-sized fan with a near-linear curve characteristic within the range of testing operating conditions. When the pressure drop increased, the flow dropped linearly, and similar behavior is expected for an actual fan-coil assembly in air-source heat pumps. It should be noted that only a small part of total airflow (about 5 cfm (0.0024 m^3/s)) was diverted to the small microchannel samples, while the rest of flow (about 100 cfm (0.047 m^3/s)) was recirculated and bypassed the fin sample. Thus, when reducing 5 cfm (0.0024 m^3/s) of the sample to 0 cfm, the rest of the flow was practically unaffected, and the working conditions of the fan in the test setup were not drastically influenced during the frosting tests of the present work. From this perspective, it was concluded that the data obtained in the present study on air face velocity reduction were practically independent from the fan used in the test setup. It was clear that the change of air velocity was mainly due to the behavior of the fins geometry during their frost buildup. It is worth emphasizing that Equations 5–12 are explicit equations that can be set up using a spreadsheet to predict the value of frost thickness and air velocity at each time during the frost period. These values can be used to calculate the instantaneous Re number for prediction of the heat transfer coefficient.

The present correlations were developed and experimentally validated within the following geometric parameters ranges for louvered folded fins of microchannel heat exchangers: 7.6 mm < Ch_w < 13 mm, 1.15 mm < Ch_h < 2.34 mm, 19 mm < Ch_d < 30 mm, and a louver angle of approximately 30°. The inlet air was at 1.7°C/0.6°C (35°F/33°F) dry-bulb/wet-bulb temperature (~82% RH), and the initial air face velocity approaching the fins was about 1.5 m/s (~296 fpm). Future studies might be required to extend the frost and velocity reduction correlation to a broader range of fin geometries and operating conditions, specifically for a larger set of ambient temperatures and humidity.

Conclusions

The present work focused on various aspects of frost formation on louvered folded fins in outdoor microchannel heat exchangers used in air-source heat pump systems. More than 90 tests with different surface temperatures were performed on 7 microchannel fin samples. The samples had a broad range of fin density, depth, and width, while the louver angle was approximately 30° for all samples. The effects of surface temperature and fin geometry on the thermal and hydraulic performance of the microchannel heat exchangers under frosting conditions were measured and discussed. This artilcle presents new correlations for frost thickness and air face velocity reduction that properly account for frosting operating conditions of seven fin geometries for microchannel heat exchangers. The developed correlations were verified for fin surface temperatures ranging from –11°C to –5°C (12°F to 23°F) and were able to predict the frost thickness and air face velocity degradation within average error of ±17.6% and ±7.7%. Correlations that predict the frost thickness and reduction of air face velocity during frosting operations can be used to calculate the instantaneous air-side Reynolds number during frosting operation of the fins, which is a fundamental parameter for predicting the heat transfer rates of the microchannel coils in quasi-steady-state frosting operating conditions.

Nomenclature

Ch_d, C_d = channel depth (air side) or coil depth [mm]
Ch_h = channel height (air side; free space between two adjacent fins [mm]
Ch_w = channel width (air side; free space between two adjacent vertical tube walls) [mm]
D_{ab} = binary diffusion coefficient of water to air (2.28*E*–5) [m^2/s]
Fo, Fo_m = mass transfer Fourier number (Equation 5) [ ]
Fs = frost number or supersaturation level of air (Equation 1) [ ]
l_l = louver length [mm]
l_p, L_p = louver pitch [mm]
$\dot{m}$ = mass flow rate [kg/s]
P_{air} = pressure of water vapor pressure in air stream [Pa]
P_{surf} = pressure of water vapor pressure in air at surface temperature [Pa]
t = frost thickness [m]
t_{fin} = fin thickness [m]
t_t = time [s]
T = temperature [°C]
V = velocity [m/s]

Greek letters

δ = dimensionless frost thickness [ ]
ω = absolute air humidity [kg/kg]

Subscripts

0 = at initial time [$t = 0$]

f = frost
s, *surf* = surface

References

AHRI. 2008. *Standard 210/240, Performance Rating of Unitary Air Conditioning and Air-Source Heat Pump Equipment*. Air Conditioning, Heating and Refrigeration Institute, Arlington, VA.

Garimella S. 2003. Innovations in energy efficient and environmentally friendly space-conditioning systems. *Energy* 28:1593–614.

Hoke, J.L., J.G. Georgiadis, and A.M. Jacobi. 2004. Effect of substrate wettability on frost properties. *Journal of Thermophysics and Heat Transfer* 18:228–35.

Hong, T. 2011. Measurements of frost growth on louvered folded fins of microchannel heat exchangers. Master thesis, Mechanical & Aerospace Engineering, Oklahoma State University, Stillwater, OK.

Hong, T., E. Moallem, L. Cremaschi, and D.E. Fisher. 2012. Measurements of frost growth on louvered folded fins of microchannel heat exchangers, Part 1: Experimental methodology. *ASHRAE Transactions* 118:Part 1, 1101–15.

Kim, J.-H., and E A. Groll. 2003. Microchannel heat exchanger defrost performance and reliability. ASHRAE Final Report 1195-RP, ASHRAE, Atlanta, GA.

Kim, M.-H., and C.W. Bullard. 2002. Performance evaluation of a window room air conditioner with microchannel condensers. *Journal of Energy Resources Technology* 124:47–55.

Kondepudi, S.N., and D.L. O'Neal. 1989. Effect of frost growth on the performance of louvered finned tube heat exchangers. *International Journal of Refrigeration* 12:151–8.

Lee, K.-S., W.-S. Kim, and T. H. Lee. 1997. A one-dimensional model for frost formation on a cold flat surface. *International Journal of Heat and Mass Transfer* 40:4359–65.

Moallem, E., L. Cremaschi, and D.E. Fisher. 2010. Experimental investigation of frost growth on microchannel heat exchangers. *International Refrigeration and Air Conditioning Conference at Purdue University West Lafayette, IN, July 12–15*.

Moallem, E., L. Cremaschi, D.E. Fisher, and S. Padhmanabhan. 2012a. Experimental measurements of the surface coating and water retention effects on frosting performance of microchannel heat exchangers for heat pump systems. *Experimental Thermal and Fluid Science* 39:176–88.

Moallem, E., T. Hong, L. Cremaschi, D.E. Fisher, and P. Deokar. 2012b. Effect of fin design on frost and defrost thermal performances of microchannel heat exchangers. ASHRAE Final Report 1589-RP (Ed.). ASHRAE, Atlanta, GA.

Moallem, E., S. Padhmanabhan, L. Cremaschi, and D.E. Fisher. 2012c. Experimental investigation of the surface temperature and water retention effects on the frosting performance of a compact microchannel heat exchanger for heat pump systems. *Experimental Thermal and Fluid Science* 39:176–88.

Moallem, E., T. Hong, L. Cremaschi, and D.E. Fisher. 2013. Experimental investigation of adverse effect of frost formation on microchannel evaporators, Part 1: Effect of fin geometry and environmental effects. *International Journal of Refrigeration* 36:1762–75.

Na, B., and R.L. Webb. 2003. A fundamental understanding of factors affecting frost nucleation. *International Journal of Heat and Mass Transfer* 46:3797–808.

Na, B., and R.L. Webb. 2004. Mass transfer on and within a frost layer. *International Journal of Heat and Mass Transfer* 47:899–911.

Padhmanabhan, S., D.E. Fisher, L. Cremaschi, and J. Knight 2008. Comparison of frost and defrost performance between microchannel coil and fin-and-tube coil for heat pump systems. *12th International Refrigeration and Air Conditioning Conference at Purdue, West Lafayette, IN*, *July 14–17.* Paper no. R2202.

Park, C.Y., and P. Hrnjak. 2007. Effect of heat conduction through the fins of a microchannel serpentine gas cooler of transcritical CO_2 system. *International Journal of Refrigeration* 30:389–97.

Sanders, C.T. 1974. The influence of frost formation and defrosting on the performance of air coolers. Ph.D. Thesis, Technische Hogeschool, Delft, Netherlands.

Shin, J., A.V. Tikhonov, and C. Kim. 2003. Experimental study on frost structure on surfaces with different hydrophilicity: Density and thermal conductivity. *ASME Journal of Heat Transfer* 125: 84–94.

Thomas, L., H. Chen, and R.W. Besant. 1999. Measurement of frost characteristics on heat exchanger fins, Part I: Test facility and instrumentation. *ASHRAE Transactions* 105:283–93.

Xia, Y., Y. Zhong, P.S. Hrnjak, and A.M. Jacobi. 2006. Frost, defrost, and refrost and its impact on the air-side thermal-hydraulic performance of louvered-fin, flat-tube heat exchangers. *International Journal of Refrigeration* 29:1066–79.

Zhang, P., and P.S. Hrnjak. 2010. Air-side performance of a parallel-flow parallel-fin (PF^2) heat exchanger in sequential frosting. *International Journal of Refrigeration* 33:1118–28.